Research Article Vol. 31, No. 21 / 9 Oct 2023 / Optics Express 35272
Optics EXPRESS

Terahertz narrowband filter metasurfaces based on bound states in the continuum

YIN LIU,[1] QIANKUN ZHANG,[1] XIAOHUA XING,[1] DIE ZOU,[1] BINGXUAN MAO,[1] JIANQUAN YAO,[1] CHUNMEI OUYANG,[1] ZHIYONG WANG,[2] AND LIANG WU[1,*]

[1]College of Precision Instrument and Optoelectronics Engineering, Tianjin University, Key Laboratory of Optoelectronics Information and Technology (Ministry of Education), Tianjin 300072, China
[2]College of Mechanical Engineering, Tianjin University, Key Laboratory of Modern Engineering Mechanics (Ministry of Education), Tianjin 300072, China
[*]wuliang@tju.edu.cn

Abstract: The electromagnetically induced transparency (EIT) effect realized by metasurfaces have potential for narrowband filtering due to their narrow bandwidth. In optics, bound states in the continuum (BIC) can produce strong localized resonances, which means that light can be trapped and stored for long periods of time to produce very high Q-factors. This has potential applications in designing highly efficient sensors and narrow bandpass filters. Here, we present two metal-flexible dielectric metasurfaces consisting of copper structures and polyimide substrates. Quasi BICs are obtained by breaking C2 symmetry of the metal structures. Resonance-captured quasi-BICs with ultra-high q-factor resonances satisfy the dark modes required to realize the EIT and couple to the bright modes in the structure to achieve narrowband filtering. The peak transmission rates are around 0.9 at 0.29 THz-0.32 THz and 0.23 THz-0.27 THz, respectively. Our results have practical implications for the realization of low-frequency terahertz communications.

© 2023 Optica Publishing Group under the terms of the Optica Open Access Publishing Agreement

1. Introduction

Electromagnetically induced transparency (EIT) has its origins in quantum realm and refers to the phenomenon of quantum destructive interference between two different excitation paths of a three-level atomic system, producing a sharp window of transparency in the broad absorption spectrum [1]. Subsequently, EIT effects were also found in metasurfaces [2–5]. The key to realizing EIT in metasurfaces is the optical near-field coupling of two resonant modes, including bright-dark mode coupling and bright-bright mode coupling [6–18]. In order to obtain an obvious EIT phenomenon, the two resonances need to have small detuning and large Q contrast [19]. In recent years, bound states in the continuum (BICs) have been shown to be an effective way to achieve high-Q resonances [20].

BICs are special electromagnetic states with frequencies in the radiative continuum but fully localized, with infinite Q-factors, uncoupled to free space [21]. The concept of BIC originated from quantum mechanics and was introduced by von Neumann and Wigner in 1929 [22]. In recent years, high-Q and multifunctional metasurfaces have attracted more and more attention [23–25]. Introducing BIC into metasurface design can open up new directions. In general, BICs can be classified into two types, symmetrically protected BIC (SP-BIC) and parametrically tuned BIC (PT-BIC) or accidental BIC. SP-BIC is typically located in system with reflection symmetry or rotational symmetry, where coupling between different modes is prohibited and the modes are fully localized in the array structure [26]. PT-BIC can be aroused by adjusting the structural parameters to produce destructive interference between different radiation patterns belonging to the same channel [27]. In fact, there is no infinite structure of periods. Therefore, affected by structure, material absorption, and other interferences, BIC is easy transformed into a quasi-BIC coupled to the radiated wave. In the works utilizing metasurface-supported BICs, SP-BICs are

#503399 https://doi.org/10.1364/OE.503399
Journal © 2023 Received 16 Aug 2023; revised 19 Sep 2023; accepted 21 Sep 2023; published 5 Oct 2023

Optics EXPRESS

easy to implement and widely used. In practical applications, the symmetry of the structures is usually broken to transform the BICs into quasi-BICs with a high Q-factor [28–32]. Currently, metasurface-supported BICs have been used in the fields of sensing [33], microantennas [34], polarization manipulation [35], image-based applications [36,37], micro-lasers [38], nonlinear optics [39], vortex optics [40,41], and filtering [42]. The reported metasurface filters operate in infrared frequency range and have a complex design methodology.

Here, we propose an effective design method for terahertz metasurface filters using BIC. Two types of metallic BIC metasurfaces are designed, one using overall structures to generate bright and dark modes, and the other using separated structures to generate bright and dark modes, respectively. The detuning of the bright and dark modes is reduced by modulation of the structural parameters to allow the coupling of the two modes to produce EIT-like effects. The designed structures are able to realize the narrow-band filtering function in the low-frequency terahertz band, and the design method is verified by experiment. Our results can contribute to the application of metasurfaces in terahertz-band communications.

2. Material and methods

In this paper, CST Microwave Studio frequency domain solver is used for simulations. In all the simulations, unit cell boundary condition is used in both x and y directions and open boundary condition is used in z direction, the terahertz wave is positive normal incidence and the spectral distribution represents the transmission results.

2.1. Double L-shaped metasurface

Figure 1(a) shows the proposed dual L-shaped terahertz narrowband filter structure, which consists of a copper unit structure deposited on a 20 μm thick polyimide substrate. Figure 1(b) shows a top view of the unit cell structure containing two centre-symmetric L-shaped metal strips made of 200 nm thick metallic copper. The dielectric constant of polyimide is 3.3 and the conductivity of copper is 5.96×10^7 S m^{-1}. The geometrical parameters of the unit cell are period P = 680 μm, lengths L_1 = 570 μm, L_2 = 290 μm, L_3 = 90 μm, metal strip gap d = 60 μm, meta strip width is W = 60 μm and asymmetry parameter g = 40 μm. In the simulation, the excitation source is set to be a TM electromagnetic wave incident from the Zmax port.

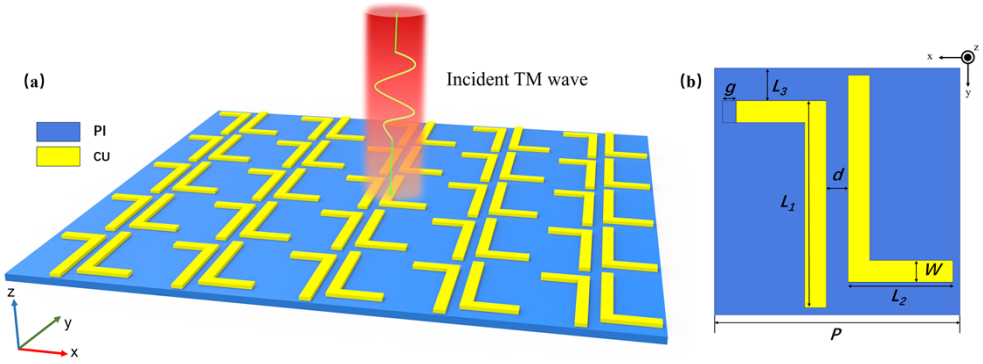

Fig. 1. (a) Schematic diagram of the proposed dual L-shaped terahertz metasurface filter (b) Front view of the cell structure with structural parameters of P = 680 μm, L_1 = 570 μm, L_2 = 290 μm, L_3 = 90 μm, d = 60 μm W = 60 μm and g = 40 μm.

The influence of the asymmetry parameter on the transmission of the structure was firstly investigated, as shown in Fig. 2(a). When the asymmetry influence factor g = 0 μm, the structure maintains C2 symmetry, at which time there is a clear dip in the transmission spectrum, and the

Optics EXPRESS

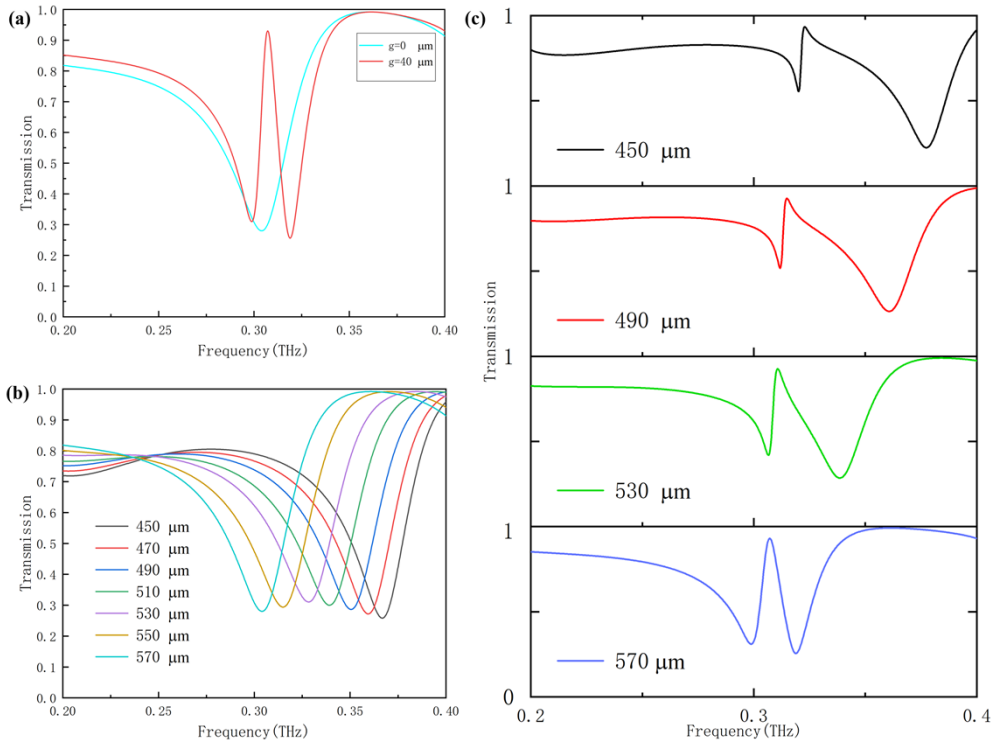

Fig. 2. (a) Effect of the asymmetry factor g (b) Transmission spectra from different L_1 at g = 0 (c) Effect from different L_1 at g = 40 μm.

lowest point of the transmission dip is located at 0.3040 THz, with a transmission rate of 0.280. When the asymmetry factor g = 40 μm, the C2 symmetry of the structure is broken, and the BIC is transformed into q-BIC. At this point, two narrower transmission dips are observed at 0.2989 THz and 0.3190 THz, with transmission rates of 0.310 and 0.256, respectively, whereas a distinct narrow-band transmission peak with a transmission rate of up to 0.930 is observed at 0.3073 THz. The full width at half maximum (FWHM) is 0.01208 THz. In order to examine the effect of the long end of the L-shaped metal strip, we simulate the transmission response of different L_1 at the asymmetry factor g = 0 μm, as shown in Fig. 2(b). Since the structure maintains C2 symmetry at this point, a significantly wider valley of resonance is observed for the intrinsic coupling resonance of the metal structure, which we call here the bright mode. The resonance valley of the bright mode appears red-shifted when L_1 is gradually increased from 450 μm to 570 μm. Further, we examined the effect of different L_1 at an asymmetry factor of g = 40 μm, as shown in Fig. 2(c). When L_1 = 450 μm, two transmission dips are generated in its transmission spectrum, and the transmission dip at the higher frequency originates from intrinsic coupling resonance of the structure, i.e., the bright mode. The transmission dip at the lower frequency position is the Fano resonance formed by the BIC leakage (q-BIC) generated by breaking symmetry of the structure, which is called the dark mode. At this time, the q-BIC occurs far away from the intrinsic coupling resonance of the structure in the transmission spectrum, and does not exhibit any obvious transmission peak. When L_1 increases, both the q-BIC and the intrinsic resonance dip positions are redshifted, but the redshift of the bright mode is faster, which can be considered as the location of the q-BIC occurrences gradually approaching the intrinsic resonance of the structure. When L_1 is increased to 570 ¼m, we consider that the bright mode is close enough to

Optics EXPRESS

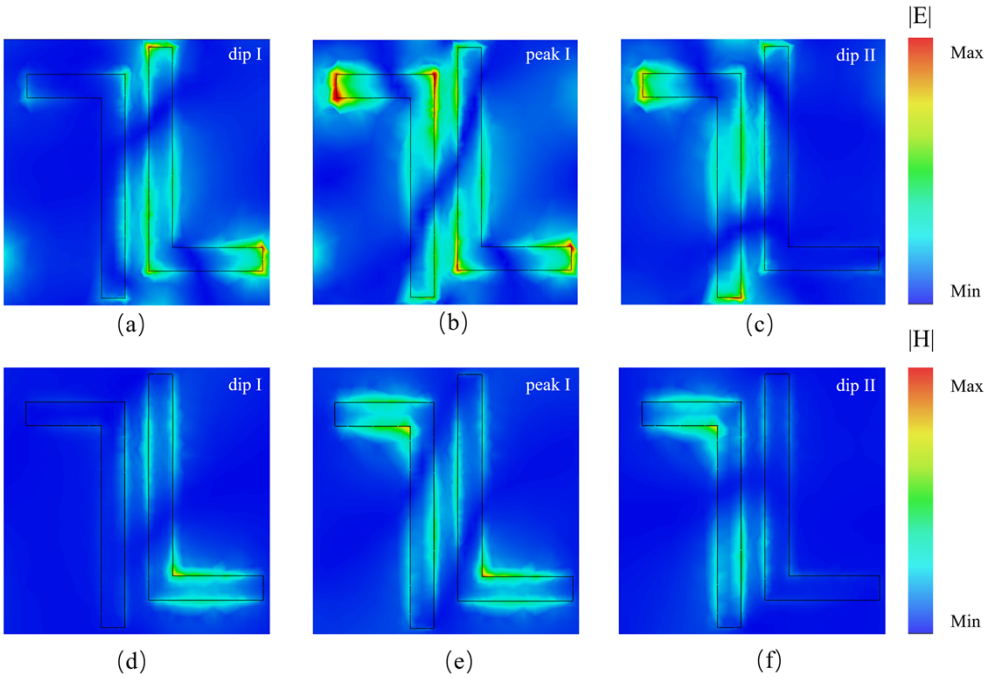

Fig. 3. Electric and Magnetic field distributions of double L-shaped metasurface (L1 = 570 μm and g = 40 μm) (a)–(c) Electric field distributions at dip I (0.2989 THz), peak I (0.3073 THz), and dip II (0.3190 THz), (d)–(f) Magnetic field distributions at dip I (0.2989 THz), peak I (0.3073 THz) and dip II (0.3190 THz).

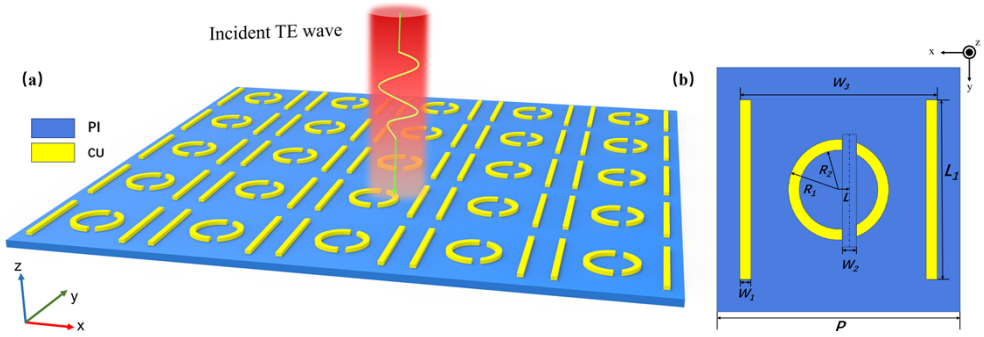

Fig. 4. (a) Schematic diagram of the proposed asymmetric open ring terahertz filter (b) Front view of the cell structure with structural parameters of P = 680 μm, L_1 = 500 μm, W_1 = 30 μm, W_2 = 40 μm, W_3 = 550 μm, d = 60 μm, R_1 = 140 μm, R_2 = 110 μm and L = 30 μm.

the dark mode, i.e., the detuning of the dark mode to the bright mode is small enough, and a clear narrow-band transmission peak can be observed at this time.

To further understand the excitation principle of the EIT-like effect here, we analyzed the E-field distribution and the M-field distribution in the x–y plane under the condition of L_1 = 570 μm and g = 40 μm at the transmission dip I (0.2989 THz), peak I (0.3073 THz), and dip II (0.3190 THz). As shown in Fig. 3(a)-(f), the localized electric and magnetic fields appear on the left and right side of the structure at dip I and dip II, respectively. According to Fig. 2(c), We consider that the localized electric and magnetic fields at dip I is induced by the BIC leakage q-BIC, while

Optics EXPRESS

the localized electric and magnetic fields at dip II is due to the intrinsic resonance of the structure brought by tuning the parameter L1. At peak I, the destructive interference of the two modes causes a sharp transmission peak with electric and magnetic fields as shown in Fig. 3(b) and (e).

2.2. Asymmetric open ring metasurface

To further illustrate this narrow-band transmission effect arisen by the coupling of bright and dark modes, we designed the following structure shown in Fig. 4. The structure consists of two symmetric metal rods and an asymmetric circular metal open ring. Same as the previous metasurface, the metal portion is copper and the substrate portion is polyimide. The metal layer thickness is 200 nm deposited on a 20 μm thick polyimide substrate. The specific parameters are $W_3 = 550$ μm, $P = 680$ μm for both x and y directions, metal bar length $L_1 = 500$ μm, metal bar width $W_1 = 30$ μm, $W_2 = 40$ μm, metal circular ring outer diameter $R_1 = 140$ μm, inner diameter $R_2 = 110$ μm, and asymmetric parameter of the metal ring $L = 30$ μm. The height of the metal structure $H_2 = 200$ nm, and thickness of the polyimide substrate is 20 μm. In the simulation, the excitation source is set to be a TE electromagnetic wave incident from the Zmax port.

In order to elucidate the formation mechanism of the narrow-band transmission, we simulated three sets of samples separately, the first sample consists of an array of metal rods, the second sample consists of an array of asymmetric metal open rings, and the third sample consists of a combination of metal rods and open rings. The transmissions of the first sample (metal rods only) and the second sample (metal asymmetric ring only) are shown in Fig. 5(a). The metal rod array structure exhibits a clear localized resonance transmission dip, reaching a minimum at 0.2458 THz. The transmission from the metal asymmetric ring exhibits a sharper narrow-band transmission dip with a centre frequency at 0.2494 THz. Further, we examined the effect brought

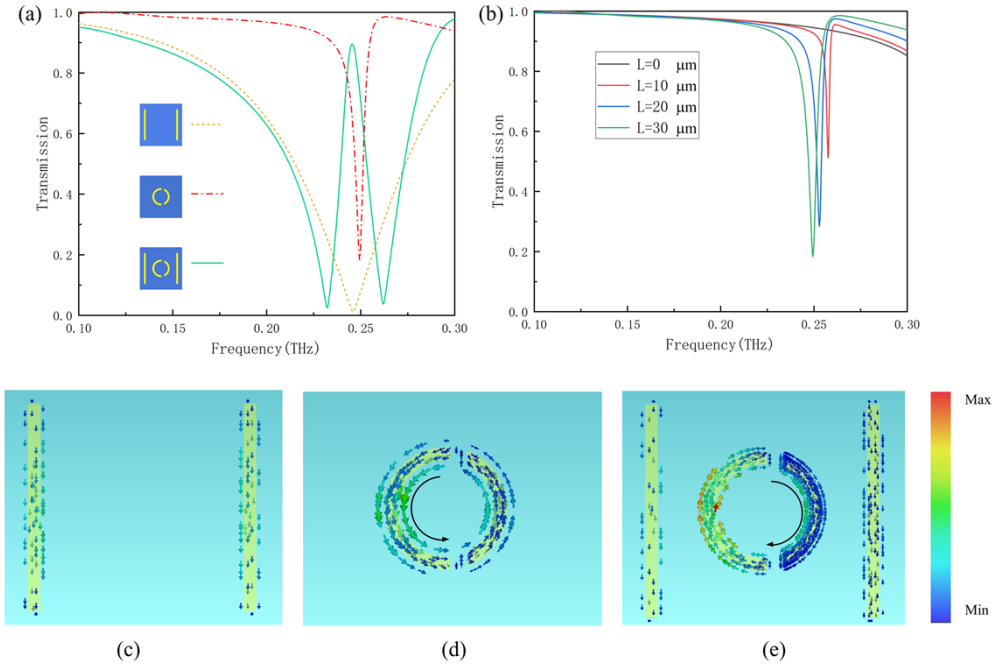

Fig. 5. (a) Transmission spectra of metal rods (earthy dashes), asymmetric open ring (red dot-dash line) and combined structure (green soild line) (b) Effect of asymmetry factor on open rings (c) Surface currents of metal rods (0.2458 THz), (d) asymmetric open ring, (0.2494 THz), (e) combined structure (0.2455 THz).

Optics EXPRESS

by the asymmetry factor of the metal ring, as shown in Fig. 5(b). When the asymmetry factor is 0, the transmission spectrum is smoother and there is no obvious transmission decline. When the asymmetry factor is gradually increased from 0 to 30, it can be seen that an obvious sharp transmission dip, i.e., q-BIC, is formed. Thus, the metal rod and the asymmetric metal open ring act as the bright and dark modes under excitation, respectively. The destructive interference of the two modes leads to the formation of a sharp transmission peak at 0.2455 THz with a FWHM of 0.01519 THz for the combined structure. Figure 5(c)-(e) simulate the surface currents of the proposed metal rods, metal open rings, and combination structures at their resonances, respectively. It's worth noting that the surface current direction of the individual metal open rings is opposite to the surface current direction of the open rings in the combined structure. It is due to the coupling of the bright mode of the metal rod to the dark mode of the open ring, which generates a reverse current and realizes the EIT effect.

A comparison of the two metasurfaces designed in this paper with [43–45] is shown in Table 1. It is worth noting that although metasurface1 (double L-shaped metasurface) has a larger Q-factor than metasurface2 (open ring metasurface), there is a more pronounced low-pass effect in metasurface 2.

Table 1. Performance comparison of previous filters with our work

Ref	f_0(THz)	Transmission	FWHM(THz)	Q-Value
[43]	0.481	0.7008	0.1766	2.725
	0.931	0.6778	0.2605	3.574
[44]	2.950	0.89	0.19	15.5
[45]	1.43	0.943	0.13	11.0
metasurface1	0.3073	0.93	0.01208	25.4
metasurface2	0.2455	0.895	0.01519	16.2

3. Experiment result and discussion

The samples were fabricated by spin-coating approximately 20 μm thick polyimide on a pre-prepared silicon substrate using a spin-coater. The preparation of the metallic portion was then completed by a mask plate. It is noteworthy that in order for the metallic copper to be able to combine with the polyimide substrate, about 10 nm thick metallic titanium needs to be fabricated between the copper and the polyimide layers, which will inevitably cause some errors in the results. Both metasurface structures presented in previous chapters were characterized by a laser scanning confocal microscope (LSCM), and the obtained microscope scanning structures are shown in Fig. 6(a) and (b).

A transmission-type terahertz time-domain spectrometer (TDS) was used for the measurements of the samples as shown in Fig. 6(c). During the experiments, the sample was removed from the silicon substrate and measured. To minimise the effect of moisture in the air on the terahertz waves, we filled the TDS system with dry air and kept the air humidity below 5%. Figures 7(a) and (c) show the comparison of terahertz time-domain and air signals for the double L-shaped metasurface and open ring metasurface, respectively. It is worth mentioning that the sample time-domain measurements obtained have almost no delay from the air time-domain measurements due to the small thickness of both the substrate and the structural part of our

Optics EXPRESS

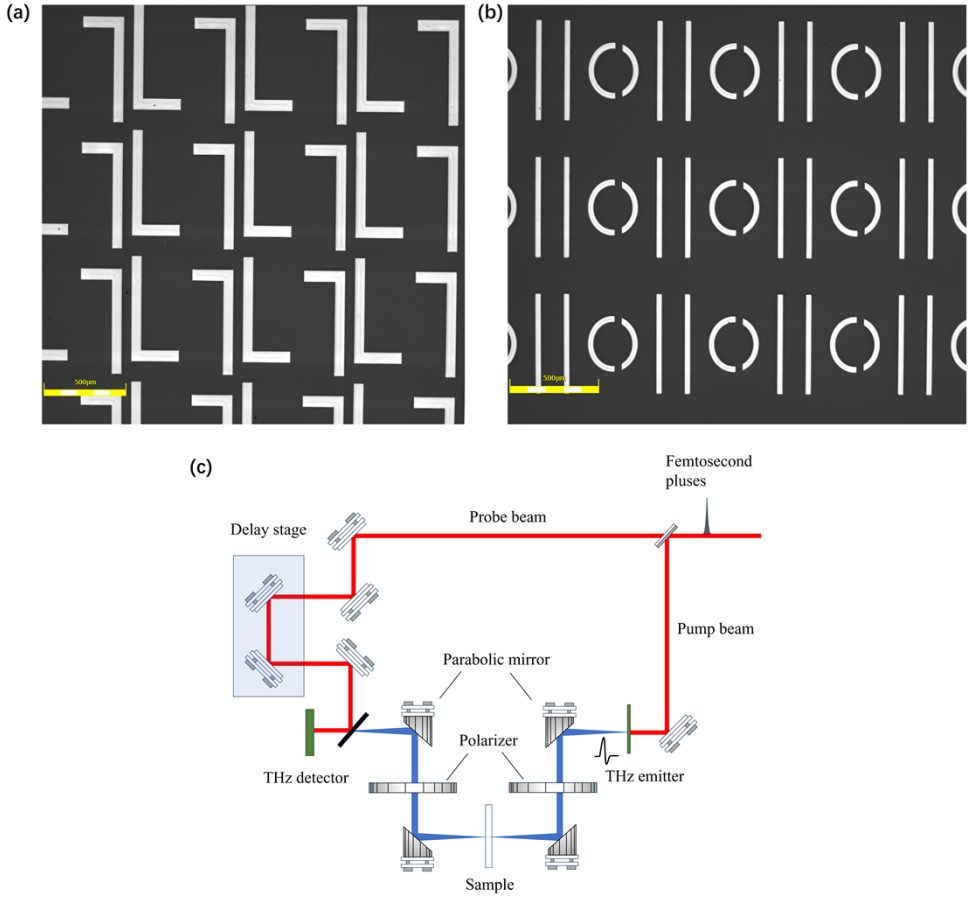

Fig. 6. Structure of (a) double L-shaped metasurface, (b) open ring metasurface obtained by LSCM scanning, (c) Schematic diagram of the THz-TDS experimental system.

measurement samples. The transmissions of the samples are obtained after Fourier transform. The comparison of the transmission obtained from the experiments and the transmission obtained from the simulations are shown in Fig. 7(b) and (d), respectively. We note a decrease in amplitude and a frequency shift between the simulated and measured transmission. The reason for this inaccuracy is the processing accuracy limitation. In addition, there are accuracy limitations in the TDS measurement system we used. Then, there's the fact that the metasurfaces operate in the low-frequency terahertz band, and the TDS system used has a low signal energy in the range of 0.1 to 0.4 THz, which is susceptible to interference. During the experiment, charging dry air will unavoidably bring airflow disturbance, as well as we can not accurately control the air humidity during the experiment, all of which will bring discrepancies to the results.

Optics EXPRESS

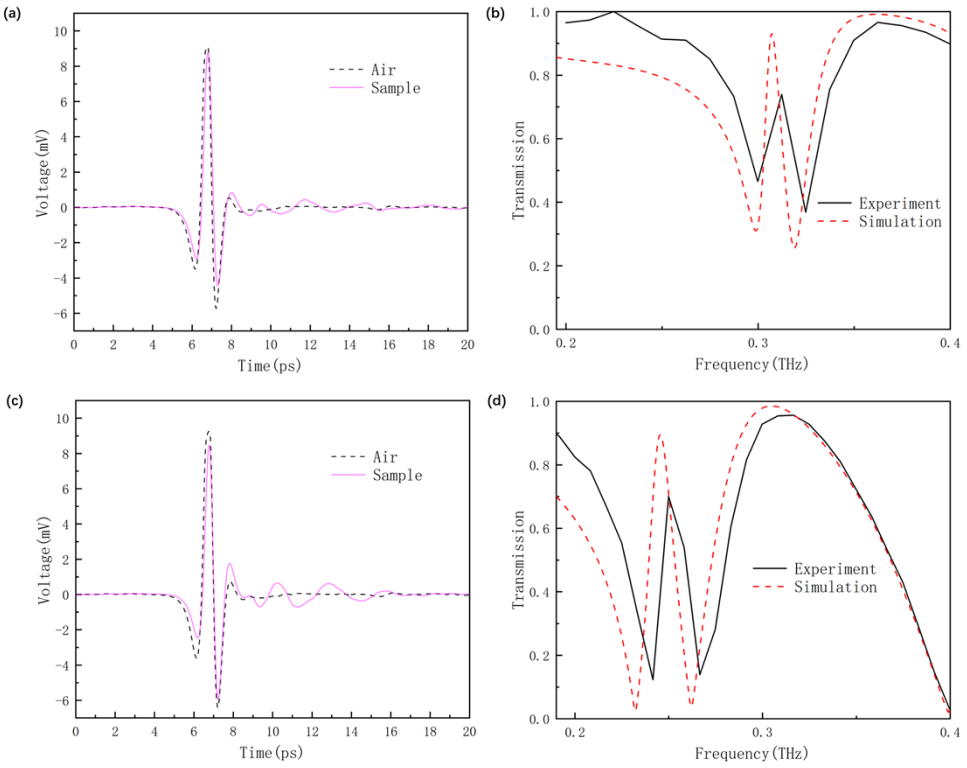

Fig. 7. Experimental results of the two types of metasurfaces (a) air vs. sample time-domain signal plots for double L-shaped metasurfaces and (b) experimental vs. simulated transmission for double L-shaped metasurfaces, (c) air vs. sample time-domain signal plots for open ring metasurfaces and (d) experimental vs. simulated transmission for open ring metasurfaces.

4. Conclusions

In summary, we have proposed a metasurface design method for narrow-band filtering using quasi-BIC, and designed two metal-flexible dielectric metasurface structures. By breaking C2 symmetry, we obtain sharp transmission peaks to achieve the narrowband filtering function. By changing the length of the metal strips and the opening position of the circular ring, BIC state becomes quasi-BIC state and a Fano-type resonance with a high Q-factor (dark mode) is excited at the terahertz frequency. At the same time, by tuning the structural parameters, the intrinsic coupling vibration (bright mode) of the structure can be modulated so that its occurrence position in the spectrum coincides with that of the dark mode. Then the further coupling of the two modes results in distinct narrow-band transmission peaks. Experimentally, we have characterized the samples by a laser confocal scanning microscope and completed the measurement of the transmission spectrum by a TDS system. The experimental results are in good agreement with the simulation results. Our work provides a new simple design method for realizing narrow-band filters on a super-surface, which has practical potential for using terahertz waves in communications.

Funding. National Key Research and Development Program of China (Grant No. 2022YFA1203500); National Natural Science Foundation of China (U2230114).

Disclosures. The authors declare no conflicts of interest.

Optics EXPRESS

Data availability. Data underlying the results presented in this paper are not publicly available at this time but may be obtained from the authors upon reasonable request.

References

1. S. E. Harris, "Electromagnetically induced transparency," Phys. Today **50**(7), 36–42 (1997).
2. N. Papasimakis, V. A. Fedotov, N. I. Zheludev, and S. L. Prosvirnin, "Metamaterial analog of electromagnetically induced transparency," Phys. Rev. Lett. **101**(25), 253903 (2008).
3. S. Zhang, D. A. Genov, Y. Wang, M. Liu, and X. Zhang, "Plasmon-induced transparency in metamaterials," Phys. Rev. Lett. **101**(4), 047401 (2008).
4. P. Tassin, L. Zhang, T. Koschny, E. N. Economou, and C. M. Soukoulis, "Low-loss metamaterials based on classical electromagnetically induced transparency," Phys. Rev. Lett. **102**(5), 053901 (2009).
5. Y. M. Yang, I. I. Kravchenko, D. P. Briggs, and J. Valentine, "All-dielectric metasurface analogue of electromagnetically induced transparency," Nat. Commun. **5**(1), 5753 (2014).
6. F. L. Zhang, Q. Zhao, J. Zhou, and S. X. Wang, "Polarization and incidence insensitive dielectric electromagnetically induced transparency metamaterial," Opt. Express **21**(17), 19675–19680 (2013).
7. J. F. Zhang, W. Liu, X. D. Yuan, and S. Q. Qin, "Electromagnetically induced transparency-like optical responses in all-dielectric metamaterials," J. Opt. **16**(12), 125102 (2014).
8. J. Hu, T. T. Lang, Z. Hong, C. Y. Shen, and G. H. Shi, "Comparison of electromagnetically induced transparency performance in metallic and all-dielectric metamaterials," J. Lightwave Technol. **36**(11), 2083–2093 (2018).
9. Y. Lu, J. Y. Rhee, W. H. Jang, and Y. P. Lee, "Active manipulation of plasmonic electromagnetically-induced transparency based on magnetic plasmon resonance," Opt. Express **18**(20), 20912–20917 (2010).
10. B. X. Han, X. J. Li, C. S. Sui, J. Y. Diao, X. F. Jing, and Z. Hong, "Analog of electromagnetically induced transparency in an E-shaped all-dielectric metasurface based on toroidal dipolar response," Opt. Mater. Express **8**(8), 2197–2207 (2018).
11. J. Y. Diao, B. X. Han, J. Yin, X. J. Li, T. T. Lang, and Z. Hong, "Analogue of electromagnetically Induced transparency in an S-shaped all-dielectric metasurface," IEEE Photonics J. **11**(3), 1–10 (2019).
12. N. Liu, L. Langguth, T. Weiss, J. Kastel, M. Fleischhauer, T. Pfau, and H. Giessen, "Plasmonic analogue of electromagnetically induced transparency at the Drude damping limit," Nat. Mater. **8**(9), 758–762 (2009).
13. X. R. Jin, J. Park, H. Zheng, S. Lee, Y. Lee, J. Y. Rhee, K. W. Kim, H. S. Cheong, and W. H. Jang, "Highly-dispersive transparency at optical frequencies in planar metamaterials based on two-bright-mode coupling," Opt. Express **19**(22), 21652–21657 (2011).
14. C. K. Chen, Y. C. Lai, Y. H. Yang, C. Y. Chen, and T. J. Yen, "Inducing transparency with large magnetic response and group indices by hybrid dielectric metamaterials," Opt. Express **20**(7), 6952–6960 (2012).
15. L. Zhu, X. Zhao, L. Dong, J. Guo, X. J. He, and Z. M. Yao, "Polarization-independent and angle-insensitive electromagnetically induced transparent (EIT) metamaterial based on bi-air-hole dielectric resonators," RSC Adv. **8**(48), 27342–27348 (2018).
16. R. Yahiaoui, J. A. Burrow, S. M. Mekonen, A. Sarangan, J. Mathews, I. Agha, and T. A. Searles, "Electromagnetically induced transparency control in terahertz metasurfaces based on bright-bright mode coupling," Phys. Rev. B **97**(15), 155403 (2018).
17. F. Y. He, B. X. Han, X. J. Li, T. T. Lang, X. F. Jing, and Z. Hong, "Analogue of electromagnetically induced transparency with high-Q factor in metal-dielectric metamaterials based on bright-bright mode coupling," Opt. Express **27**(26), 37590–37600 (2019).
18. J. F. Algorri, D. C. Zografopoulos, A. Ferraro, B. Garcia-Camara, R. Beccherelli, and J. M. Sanchez-Pena, "Ultrahigh-quality factor resonant dielectric metasurfaces based on hollow nanocuboids," Opt. Express **27**(5), 6320–6330 (2019).
19. B. Luk'Yanchuk, N. I. Zheludev, S. A. Maier, N. J. Halas, P. Nordlander, H. Giessen, and C. T. Chong, "The fano resonance in plasmonic nanostructures and metamaterials," Nat. Mater. **9**(9), 707–715 (2010).
20. C. W. Hsu, B. Zhen, A. D. Stone, J. D. Joannopoulos, and M. Soljačić, "Bound states in the continuum," Nat. Rev. Mater. **1**(9), 16048 (2016).
21. E. N. Bulgakov and A. F. Sadreev, "Bound states in the continuum in photonic waveguides inspired by defects," Phys. Rev. B **78**(7), 075105 (2008).
22. J. von Neumann and E. P. Wigner, "Uber merkwürdige diskrete eigenwerte," Phys. Z. **30**, 291–293 (1929).
23. J. Qu, H. Pan, Y. Z. Sun, and H. F. Zhang, "Multitasking Device Regulated by the Gravity Field: Broadband Anapole-Excited Absorber and Linear Polarization Converter," Ann. Phys. (Berlin, Ger.) **534**(9), 2200175 (2022).
24. D. X. Wang, K. D. Xu, S. Y. Luo, Y. Q. Cui, L. Y. Zhang, Z. Liao, and J. L. Cui, "Dual-band terahertz absorber based on square ring metamaterial structure," Opt. Express **31**(4), 5940–5950 (2023).
25. D. X. Wang, K. D. Xu, S. Y. Luo, Y. Q. Cui, L. Y. Zhang, and J. L. Cui, "A high Q-factor dual-band terahertz metamaterial absorber and its sensing characteristics," Nanoscale **15**(7), 3398–3407 (2023).
26. K. Koshelev, S. Lepeshov, M. Liu, A. Bogdanov, and Y. Kivshar, "Asymmetric Metasurfaces with High-Q Resonances Governed by Bound States in the Continuum," Phys. Rev. Lett. **121**(19), 193903 (2018).
27. J. T. Li, J. Li, C. Zheng, Z. Yue, S. Wang, M. Li, H. Zhao, Y. Zhang, and J. Yao, "Free switch between bound states in the continuum (BIC) and quasi-BIC supported by graphene-metal terahertz metasurfaces," Carbon **182**, 506–515 (2021).

Optics EXPRESS

28. C. Zhou, X. Qu, S. Xiao, and M. Fan, "Imaging through a fano-resonant dielectric metasurface governed by quasi–bound states in the continuum," Phys. Rev. Applied **14**(4), 044009 (2020).
29. J. Wang, J. Kühne, T. Karamanos, C. Rockstuhl, S. A. Maier, and A. Tittl, "All-dielectric crescent metasurface sensor driven by bound states in the continuum," Adv. Funct. Mater. **31**(46), 2104652 (2021).
30. K. Koshelev, Y. Tang, K. Li, D.-Y. Choi, G. Li, and Y. Kivshar, "Nonlinear metasurfaces governed by bound states in the continuum," ACS Photonics **6**(7), 1639–1644 (2019).
31. S. Campione, S. Liu, L. I. Basilio, L. K. Warne, W. L. Langston, T. S. Luk, J. R. Wendt, J. L. Reno, G. A. Keeler, I. Brener, and M. B. Sinclair, "Broken symmetry dielectric resonators for high quality factor fano metasurfaces," ACS Photonics **3**(12), 2362–2367 (2016).
32. L. Cong and R. Singh, "Symmetry-protected dual bound states in the continuum in metamaterials," Adv. Opt. Mater. **7**(13), 1900383 (2019).
33. S. Romano, G. Zito, S. Torino, G. Calafiore, E. Penzo, G. Coppola, S. Cabrini, I. Rendina, and V. Mocella, "Label-free sensing of ultralow-weight molecules with all-dielectric metasurfaces supporting bound states in the continuum," Photon. Res. **6**(7), 726 (2018).
34. R. Colom, F. Binkowski, F. Betz, Y. Kivshar, and S. Burger, "Enhanced Purcell factor for nanoantennas supporting interfering resonances," Phys. Rev. Research **4**(2), 023189 (2022).
35. T. Shi, Z. L. Deng, G. Geng, X. Zeng, Y. Zeng, G. Hu, A. Overvig, J. Li, C. W. Qiu, A. Alu, Y. S. Kivshar, and X. Li, "Planar chiral metasurfaces with maximal and tunable chiroptical response driven by bound states in the continuum," Nat. Commun. **13**(1), 4111 (2022).
36. A. Tittl, A. Leitis, M. K. Liu, F. Yesilkoy, D. Y. Choi, D. N. Neshev, Y. S. Kivshar, and H. Altug, "Imaging-based molecular barcoding with pixelated dielectric metasurfaces," Science **360**(6393), 1105–1109 (2018).
37. A. Leitis, A. Tittl, M. K. Liu, B. H. Lee, M. B. Gu, Y. S. Kivshar, and H. Altug, "Angle-multiplexed all-dielectric metasurfaces for broadband molecular fingerprint retrieval," Sci. Adv. **5**(5), eaaw2871 (2019).
38. A. Kodigala, T. Lepetit, Q. Gu, B. Bahari, Y. Fainman, and B. Kante, "Lasing action from photonic bound states in continuum," Nature **541**(7636), 196–199 (2017).
39. L. Carletti, K. Koshelev, C. De Angelis, and Y. Kivshar, "Giant Nonlinear Response at the Nanoscale Driven by Bound States in the Continuum," Phys. Rev. Lett. **121**(3), 033903 (2018).
40. C. Huang, C. Zhang, S. Xiao, Y. H. Wang, Y. B. Fan, Y. L. Liu, N. Zhang, G. Y. Qu, H. J. Ji, J. C. Han, L. Ge, Y. Kivshar, and Q. H. Song, "Ultrafast control of vortex microlasers," Science **367**(6481), 1018–1021 (2020).
41. B. Wang, W. Liu, M. Zhao, J. Wang, Y. Zhang, A. Chen, F. Guan, X. Liu, L. Shi, and J. Zi, "Generating optical vortex beams by momentum-space polarization vortices centred at bound states in the continuum," Nat. Photonics **14**(10), 623–628 (2020).
42. J. M. Foley, S. M. Young, and J. D. Phillips, "Symmetry-protected mode coupling near normal incidence for narrow-band transmission filtering in a dielectric grating," Phys. Rev. B **89**(16), 165111 (2014).
43. Y. Zhang, D. X. Yang, D. Zhao, D. N. Hao, P. G. Zhou, Y. M. Ren, L. I. Rui, D. Zhu, Fei Fan, G. Chang, R. Moro, and L. Ma, "Dual-frequency switchable bandpass filter in the terahertz range based on enhanced trapped-mode resonances," Chem. Phys. Lett. **826**, 140637 (2023).
44. M. Zhong, "Realization of terahertz single-band metamaterial filter based on the bright-bright coupling," Opt. Mater. (Amsterdam, Neth.) **105**, 109914 (2020).
45. H. B. Xu, "Design, simulation and measurement of a single-band high-transmittance all-dielectric metamaterial filter," Opt. Mater. (Amsterdam, Neth.) **125**, 112145 (2022).

210.28.140.4 {ts '2023-10-31 09:23:58'}